2020

Track Multiplicity and Its Potential as a Probe into Supersymmetry

Elise Chavez

The Florida State University
College of Arts and Sciences

Track Multiplicity and Its Potential as a Probe into Supersymmetry

By

Elise Chavez

A Thesis submitted to the Department of Physics in partial fulfillment of the requirements for graduation with Honors in the Major

Degree Awarded:
Spring, 2020

The members of the Defense Committee approve the thesis of Elise Chavez defended on April 13^{th}, 2020.

Dr. Andrew Askew
Thesis Director

Dr. Matthew Moore
Outside Committee Member

Dr. Laura Reina
Committee Member

Abstract

This thesis presents a viability study for the use of track multiplicity ξ as a tool in background analysis for various types of searches. In essence, this work strives to understand the use of such a variable in aiding with some of the problems with searches of this kind. The test was done using the 2018 CMS data at $\sqrt{s}$= 13 TeV where the data used had an integrated luminosity of $54.67 fb^{-1}$. In the end, the test for feasibility was inconclusive. Track multiplicity was shown to be a variable of potential, but did not give a conclusive answer to the search for dark matter. ξ distributions were made for three regions, candidate sample, electron control, and $W\gamma$ region, in slices of transverse momentum using information from jets. The shapes were then compared.

Contents

List of Figures

List of Tables

1 Introduction

1.1 Supersymmetry and Dark Matter

The standard model of particle physics is an incredibly useful and successful description of the subatomic world. In it are all of the experimentally observed particles that make up the visible universe. These particles are categorized into fermions and bosons, where fermions have half integer spin and bosons have integer spin. The scalar Higgs-boson is an exception as it has a spin of 0. While it has served physicists well, this version of standard model is not complete as there are still many pressing questions left to answer. One such question concerns the existence of dark matter. Dark matter was observed cosmologically when the rotation of galaxies were shown to be influenced by some extra matter invisible to any current detection methods. However, there is no dark matter particle in the current standard model indicating that, though it is a good description of the universe, it is not perfect.

Supersymmetry, a theory with many answers but elusive evidence, has been long searched for by particle physicists as an answer to this question of dark matter. It proposes supersymmetric partners to the experimentally observed standard model particles. For example, the electron would have a bosonic partner called the selectron. At the same time, one of these theorized particles could be a dark matter candidate under R-parity conserving supersymmetry (SUSY). R-parity is essential here because it guarantees that the lightest supersymmetric particle cannot decay which is needed for a dark matter candidate. It ensures that standard model processes must produce even numbers of supersymmetric particles which in turn can only decay to odd numbers of supersymmetric particles. Thus implying the lightest one cannot decay. These supersymmetric partners have yet to be discovered despite extensive searches for them. But, if found, SUSY could begin to complete the standard model and physicists current understanding of the universe. For some models of SUSY, searches have excluded much of the parameter space where SUSY could exist, with mass limits being placed on these model dependent supersymmetric particles. However, there are still many models to explore and thus much of parameter space to probe given the appropriate methods and tools. The focus of this work is to explore a novel way to search for SUSY, in particular low-mass splitting SUSY, by employing track multiplicity as a variable of interest. This method has not yet been attempted experimentally but has been previously proposed[1].

This term low-mass splitting supersymmetry refers to a process where the production of a supersymmetric particle is masked by a small mass difference between it and its immediate parent. This means that when the visible energy, which is low, is analyzed, it is very difficult to infer that a supersymmetric particle was produced and escaped. The low mass difference makes it very difficult to distinguish the supersymmetric particle and quantum chromodynamic (QCD) multijet events.

1.2 Methodology and Event Signature

For this particular type of supersymmetry, there has been a need to develop a better method of analysis. The method of utilizing track multiplicity of the final state particles was proposed to deal with the hardships of searching for low-mass splitting SUSY. To deal with these hardships, and the fact that it is hard to distinguish from QCD, the track multiplicity ξ will be used to analyze the data. Track multiplicity is much more sensitive to these low-mass splitting events as it is largely uncorrelated to the usual variables of analysis. For this analysis, the final state will be a single photon emitted as initial state radiation and missing transverse energy. The difficulty here is that the rate of production of real single photons is large.

The data that will be used is most of the 2018 data using the single photon trigger. The integrated luminosity for this is 54.67 fb^{-1}. A trigger is what tells the computers which events to record from the collision data as the collisions are occurring. This is essential because the LHC produces more data than can be written. The 2018 single photon trigger is a new trigger that has only recently been implemented, which is part of why this proposed method can practically be attempted. It is one of several of its kind, but it attempts to trigger only on events that produce a single photon with energies as low as 110 GeV.

This search involves triggering on the single photon that is emitted by an initial state quark, which is termed initial state radiation, more specifically $p + p \rightarrow \chi_2\bar{\chi_2} \rightarrow qqqq\chi^0\chi^0 + \gamma$. The signature of the desired events will thus be a single photon and missing transverse energy. The background for such events largely come from the decay of Z and $\text{W}^{\pm}$ bosons. For the Z, the decay is $\text{Z}\gamma \rightarrow \nu\nu\gamma$ and for the $\text{W}^{\pm}$, the decay is $\text{W}^{\pm}\gamma \rightarrow l\nu\gamma$. In either case, they also produce the photon plus missing transverse energy final state and they make up approximately three-fourths of the potential background [3]. A large part of this project is modeling this background which will be done by using what are termed Drell-Yan events. These are events where two quarks annihilate to produce a lepton and an anti-lepton in the final state. They closely mimic the Z boson decay to a photon and a neutrino/anti-neutrino once lepton tracks are removed from events where there are charged leptons in the final state of the boson decay. The background for both will be analyzed using track multiplicity in order to determine the viability of the use of track multiplicity, denoted ξ, as an analysis tool. The use of track multiplicity here should be a useful test as there is a cascade decay of squarks in the dark matter production meaning greater number of tracks. Thus, ξ is expected to be different for the SUSY event and the electroweak backgrounds. For this method to be viable, track multiplicity must give the ability to distinguish the electroweak background from the candidate sample, thus allowing for conclusions to be made about the candidate sample.

2 Relevant Variables

Before the detector, it is useful to discuss some of the variable used in this analysis that will be referenced throughout. The first of the types of variables are detector/spatial variables. They are η, ϕ, and ΔR. η and ΔR are defined through Equations (1) and (2), respectively.

$$\eta = -\ln(\tan(\frac{\theta}{2})) \tag{1}$$

$$\Delta R = \sqrt{(\Delta\phi)^2 + (\Delta\eta)^2} \tag{2}$$

A diagram of the coordinate system is given in Figure 1 below.

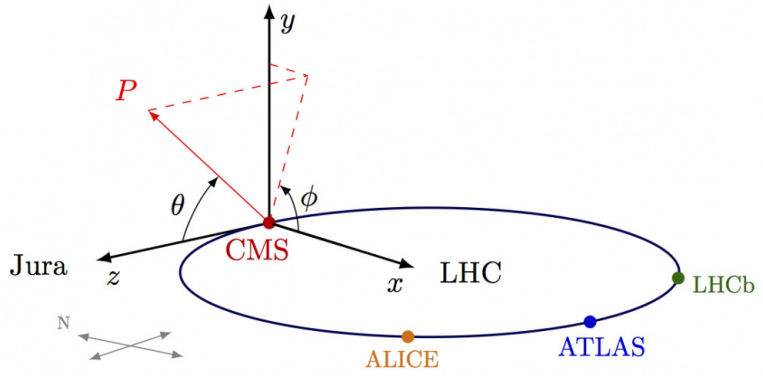

Figure 1: A diagram of the CMS coordinate system [8].

Here, θ is the polar angle and ϕ is the azimuthal angle.

Two variables that will be mentioned come from particle flow. Particle flow is a complicated algorithm used to determine the identity of particles and various properties of the collisions that are occurring. The first variable is known as missing transverse energy denoted in the paper as E_t^{miss}, it is the particle flow missing energy in the transverse direction. This is the energy calculated perpendicular to the beam line. Further, E_t^{miss} has direction that is inferred from the imbalance direction in ϕ that indicates where this energy points relative to the beam line. It is called pfMETPhi.

Further there are two more equations that should be known for this analysis. They are the equations for the invariant mass and the transverse mass. The invariant mass is the mass between two objects using their energies and momenta. It will be denoted M_{inv}, and it is defined in Equation (3) below.

$$M_{inv} = \sqrt{(E_1 + E_2)^2 - (\vec{p_1} + \vec{p_2})^2} \tag{3}$$

The transverse mass, denoted M_{trans} here, is slightly different. It keeps the same form but takes only the momenta in the x-y plane from Figure 1. In addition, the transverse mass is calculated with the second object being the missing transverse energy. This

means we take E_t^{miss} in the x and y and the particle's momentum in x and y. The energy used is simply the transverse energy of the desired particle.

The rest of the variables are defined in the tables below. Table 1 refers to photons, Table 2 refers to electrons, and Table 3 refers to both muons and jets. In addition, missing energy in the transverse direction is denoted E_t^{miss}, electrons e, photons γ, and muons μ.

Variable	Definition
N_{pho}	Number of photons
η_{pho}	photon η
ϕ_{pho}	photon ϕ
$\Delta\phi_{pho}$	Difference in ϕ between a candidate photon and pfMETphi
$PixelSeedMatch(PSM)$	Whether or not a photon has been matched to a pixel seed, this quantity is 0 if there is none and indicates a photon candidate
$ParticleFlowChargedIsolation(I_{Ch})$	Sum of the transverse momentum of the particle flow charged hadrons associated with the primary vertex(the point of interaction) within the vicinity of the photon
$ParticleFlowNeutralIsolation(I_{Neu})$	Sum of transverse energy of the particle flow neutral hadrons within the vicinity of the photon
$ParticleFlowPhotonIsolation(I_{pho})$	Sum of transverse energy of the particle flow photons within the vicinity of the photon
H/E	Ratio of the energy deposited in the closest hadronic calorimeter (HCal) tower to the position and the energy deposited in the ECAL to that position
$E_{t,pho}$	Transverse energy of the photon
$P_{t,pho}$	Transverse momentum of the photon
$\sigma_{i\eta i\eta}$	Square root of the variance of the energy distribution in a 5x5 about the seed crystal

Table 1: This table provides all necessary variable definitions for photons.

Variable	Definition
N_{ele}	Number of electrons
$PixelSeedMatch(PSM)$	Whether or not a particle has a been matched to a pixel seed, this quantity is nonzero if there is a match and indicates an electron candidate
η_{ele}	η of the electron
ϕ_{ele}	ϕ of the electron
$P_{t,ele}$	Transverse momentum of the electron

Table 2: This table provides all necessary variable definitions for electrons.

Variable	Definition
N_{jets}	Number of jets
N_{μ}	Number of muons
η_{μ}	η of the muon
ϕ_{μ}	ϕ of the muon
$P_{t,\mu}$	Transverse momentum of the electron
$P_{t,jet}$	Transverse momentum of the jet
$jetdelphi$	Difference in ϕ between a jet and pfMET
N_{CH}	Number of charged hadrons in a jet
Leading track P_t	P_t of the leading track within a jet
ξ	Number of leading jet tracks

Table 3: This table provides all necessary variable definitions for muons and jets.

These are all the relevant variables that will be referenced in this analysis, there are many but each is either used in refining the data or in selecting the candidate sample. The candidate sample is the particles that meet the requirements of photon identification and the goals of this analysis. They will also be used to select the control regions, which are regions selected in attempt to validate the method of choice. The candidate selection and control regions are defined in the following section.

3 The Compact Muon Soleniod (CMS)

The data used for this search comes from the Compact Muon Solenoid (CMS), depicted in Figure 2 located at the Large Hadron Collider (LHC) in Geneva, Switzerland. The LHC has a collision energy of 13 TeV and is the most powerful collider in the world.

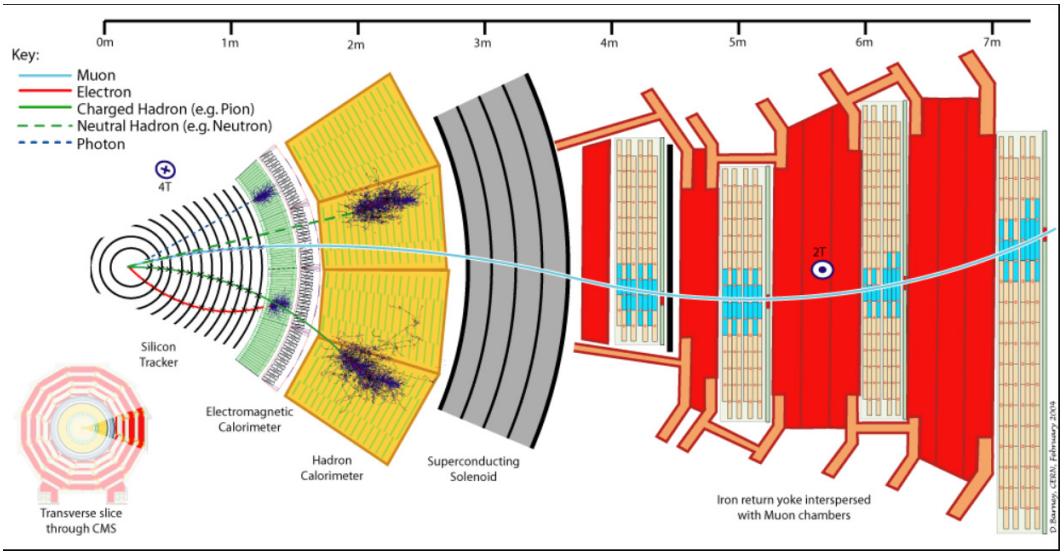

Figure 2: A diagram of a slice of the CMS experiment in the transverse plane, labeled by sub-detector [4].

3.1 The Sub-Detectors

The two most relevant sub-detectors for this study are the Silicon Tracker and the ECAL. The tracker is aptly used for the track multiplicity and the ECAL is used to detect electromagnetic objects such as electrons and photon. Working outward, the silicon tracker is composed of two parts: the silicon pixels and the silicon strips. The pixel detector is depicted in Figure 3 below.

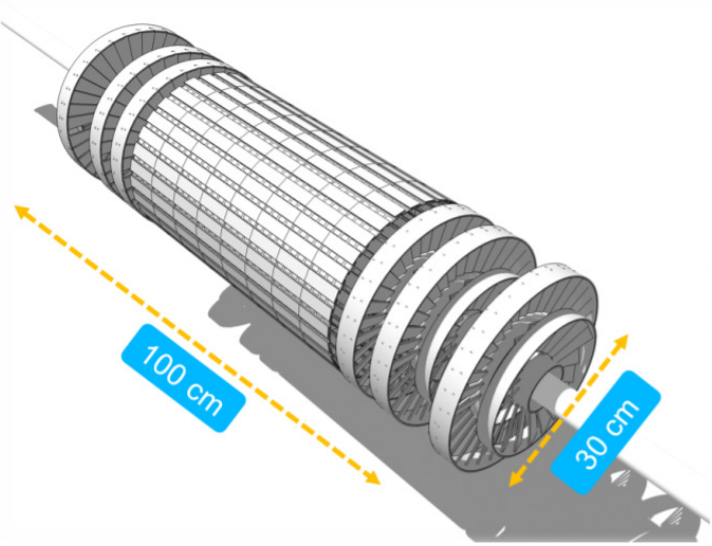

Figure 3: A depiction of the pixel detector [5].

The first part of the tracker a particle encounters is the pixel detector, which is made up of layers of silicon tiles that emit an electrical signal as a charged particle travels through. These signals are used to recreate the tracks of particles created in the beam pipe. After the pixel detector, the charged particle encounters the silicon strips. These are cylindrical shells of strips that perform similarly to the pixel detector. Together, the two sub-detectors produce data that is used to reconstruct the tracks of particles which is essential to this study.

Next is the ECAL, which is used to detect photons and electrons that are produced. The ECAL does this through the use of scintillating crystals which produce light when either an electron or photon interacts with it. A picture of the ECAL is given below in Figure 4.

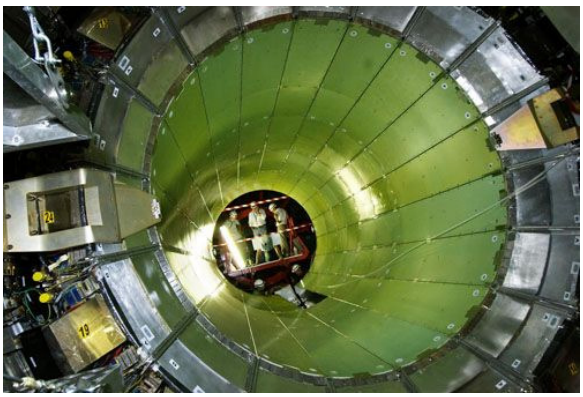

Figure 4: An image of the ECAL during construction [6].

These scintillating crystals are lead tungstate crystals. They produce light as photons or electrons trigger electromagnetic showers within them. These showers come from both the decay of the photon to two electrons that emit photons and the electrons emitting photons as it travels in the crystal. The photons, electrons, and other charged particles leave energy deposits in the ECAL. These help with tracks and identification of various particles. A depiction of the way particles leave showers in the detector are given below in Figure 5.

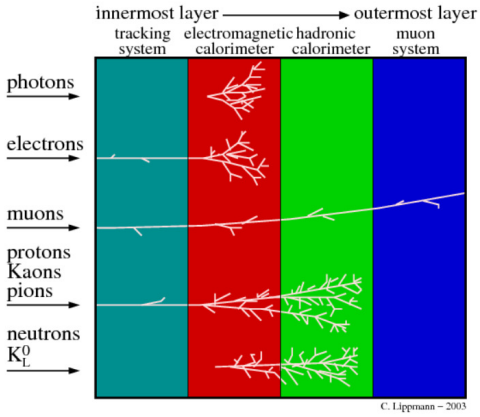

Figure 5: A diagram of how various particles leave showers or tracks in the various detectors [7].

After the ECAL, comes the Hadronic calorimeter (HCAL). The HCAL is used to detect hadrons which are particles made of quarks. It is also used to indirectly measure neutrinos. Instead of scintillating crystals, the HCAL uses scintillating plastic and an absorber to measure energy and detect particles. The absorber and plastic are layered and when the amount of light is summed up over a region of the layers, this region is called a tower.

The tracker, ECAL, and HCAL are then encased by the superconducting solenoid from which the CMS experiment gets its last initial. After the solenoid are the muon chambers interspersed with iron return yokes for the solenoid. The muon chambers are big detectors at the very edge of the experiment as muons can travel through several meters of iron without detection, as such they are rarely detected by the calorimeters. The muon chambers consist of drift tubes and cathode strip chambers. These chambers give the CMS its middle initial.

4 Candidate Selection and Control Regions

A note about both the candidate and control regions: for both a section of the data had to be removed in order to make them more equal to each other. The region is defined by $-0.02 < \eta < 1.18$ and $0.48 < \phi < 0.80$. An excess of candidate photons was noticed paired with a lack of electrons from the electron control in this region. Thus, it was excluded in these samples as it indicated some pixel inefficiency. The original η-ϕ distributions are given in Appendix A.

4.1 Candidate Selection

There are many parts to the candidate selection done for this analysis. The first part is done by algorithms performed by the trigger. In order for an event to even be considered, it must pass the HLT_Photon110EB_TightID_TightIso_v* trigger. The second is requiring that the photons are in the barrel, this means $|\eta| < 1.44$. The third part is requiring that the lead photon (photon with the highest $P_{t,pho}$) passes the medium photon identification, which is defined in Table 4, for Run 2. The next round of selection comes from the desired signature itself, where there are requirements on several different variables. We require that our photon candidate is far from E_t^{miss} in ϕ and high in P_t. Further, we require high E_t^{miss} as stipulated in the introduction. Lastly, we require that any jet is $\Delta\phi_{jet} > 0.5$ away from the missing transverse momentum $pfMET$. The final rounds of cuts are related to the jets, electrons, and muons in the event. It must be ensured that none of these objects are close to the candidate photon as this can cause misidentification and extra contributions from unwanted background. All of these cuts are summarized in Table 5 below, along with the number of events that passed.

Medium Photon Id	Cut
H/E	< 0.035
$\sigma_{i\eta i\eta}$	< 0.0103
I_{Ch}	< 1.416
I_{Neu}	$< 2.491 + 0.0126 * P_{t,pho} + 0.000026 * P_{t,pho}^2$
I_{pho}	$< 2.952 + 0.0040 * P_{t,pho}$

Table 4: Medium Photon Identification

Cut	Number of events
$P_{t,pho} > 120GeV$	25449400
In the Barrel, Eta, and Phi	24522373
$delphi > 0.5$	20941728
$E_t^{miss} > 110GeV$	433379
PSM = 0	229094
Passes Medium ID	123256
$P_{t,pho}/E_t^{miss} < 1.4$	76153
Jets	6780
Vetoes	5570
Candidates	5300

Table 5: Summary of cuts, and cut flow table for candidate events

For these photon candidates, the following plots display the distributions for their transverse energies, transverse masses, and η/ϕ. The transverse energies are given in Figure 6, the transverse masses in Figure 7, and the η-ϕ distribution in Figure 8.

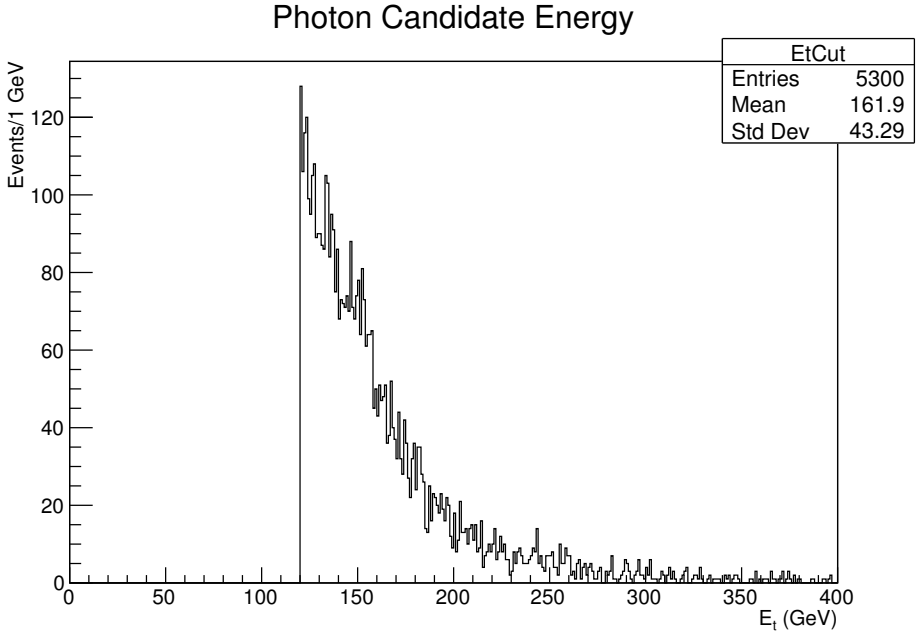

Figure 6: The E_t distribution of the photon candidates.

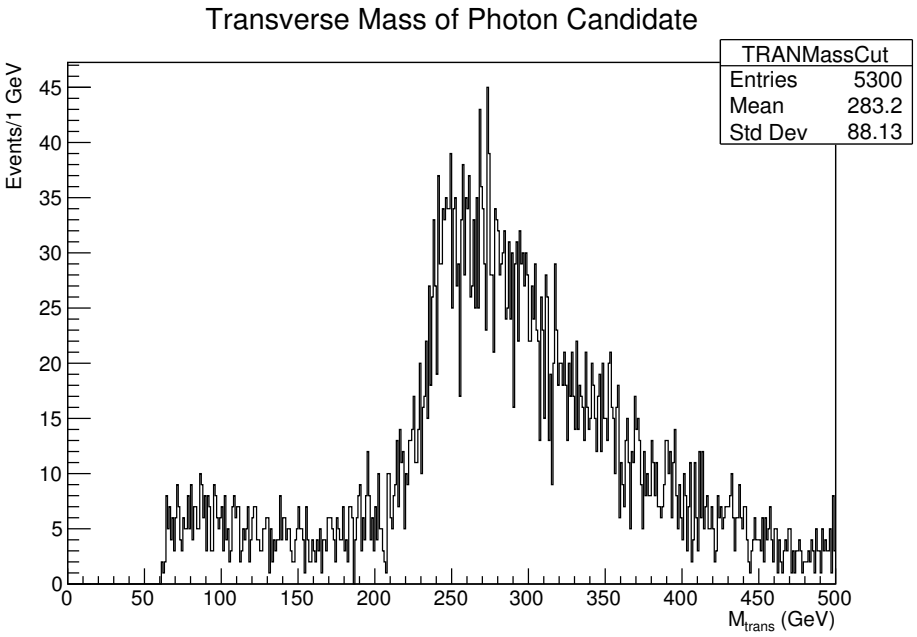

Figure 7: The M_{trans} distribution of the photon candidates.

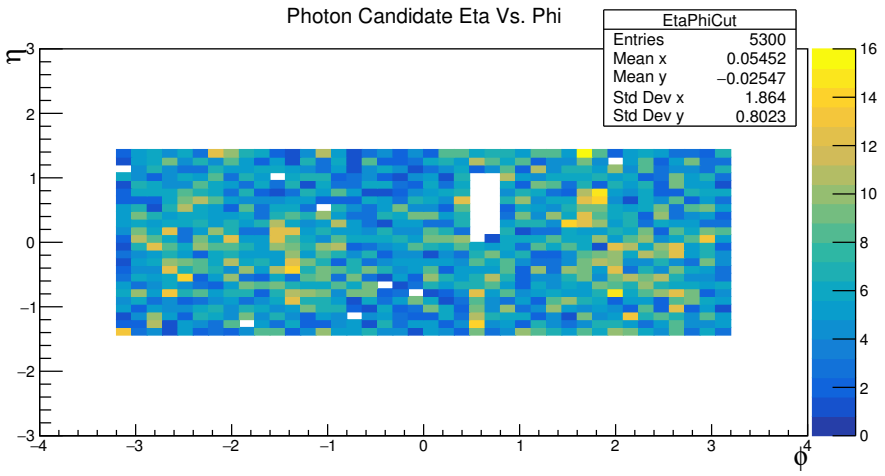

Figure 8: The η-ϕ distribution of the photon candidates.

4.2 Control Regions

Now that the candidate sample has been defined, it is necessary to compare this to control regions. These are statistically disjoint data samples that can show ξ distributions from non-SUSY events. The three regions of interest here are an electron control, a $Z \to ee\gamma$ control, and a $W\gamma \to e\nu\gamma$ control.

4.2.1 Electron

The selection for this region is identical to the candidate selection, except for the pixel seed match. For the electron control, the pixel seed match is required to be non-zero. This is a way to constrain that the photon is actually an electron, but it is still only an electron candidate. The cuts and cut flow table are given in Table 6 below.

Cut	Number of events
$P_{t,pho} > 120GeV$	25449400
In the Barrel, Eta, and Phi	24522373
$delphi > 0.5$	20941728
$E_t^{miss} > 110GeV$	433379
PSM is non-zero	204285
Passes Medium ID	127753
$P_{t,pho}/E_t^{miss} < 1.4$	103738
Jets	24491
Vetoes	20989
Electron Control	20782

Table 6: Summary of cuts, and cut flow table for Electrons

For these electron candidates, the following plots display the distributions for their transverse energies, transverse masses, and η/ϕ. The transverse energies are given in Figure 9, the transverse masses in Figure 10, and the η-ϕ distribution in Figure 11. It is worth mentioning the unique structure of the transverse mass plot, Figure 10 below. It is characteristic of the transverse mass plot for electrons with the first peak at 80-90 GeV and a secondary peak at 250-280 GeV. The first peak originates form on shell W bosons and the second peak from kinematic cuts.

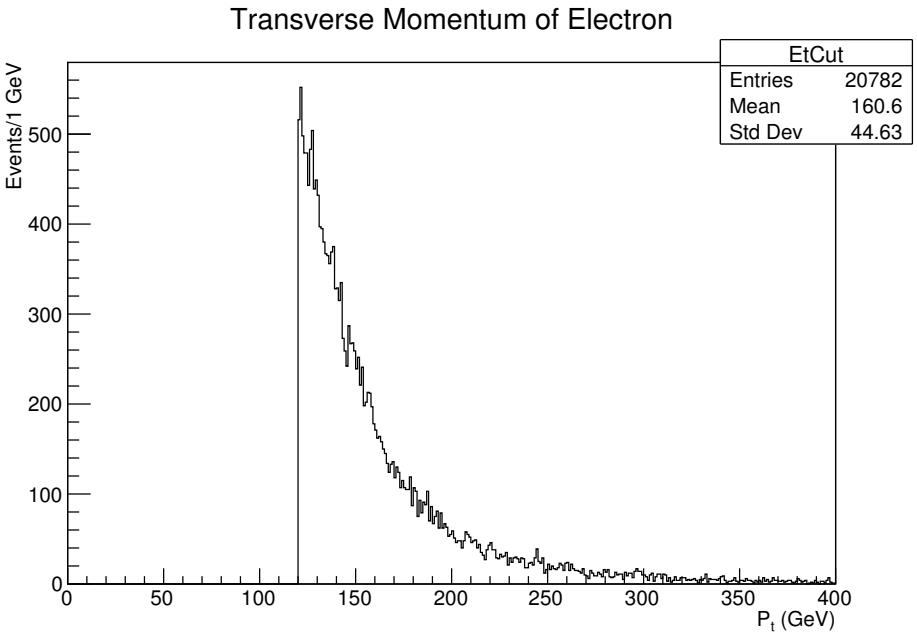

Figure 9: The E_t distribution of the electron candidates.

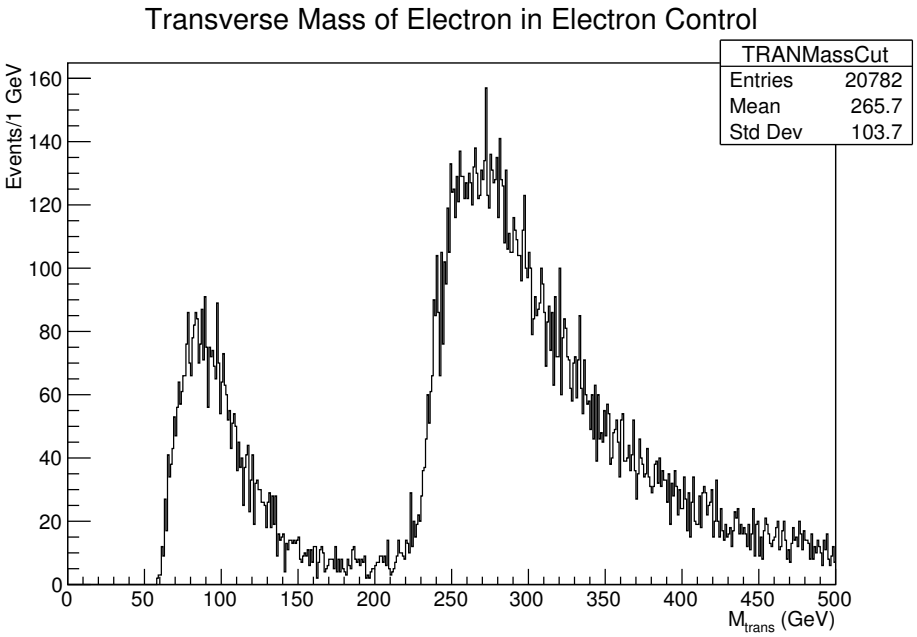

Figure 10: The M_{trans} distribution of the electron candidates.

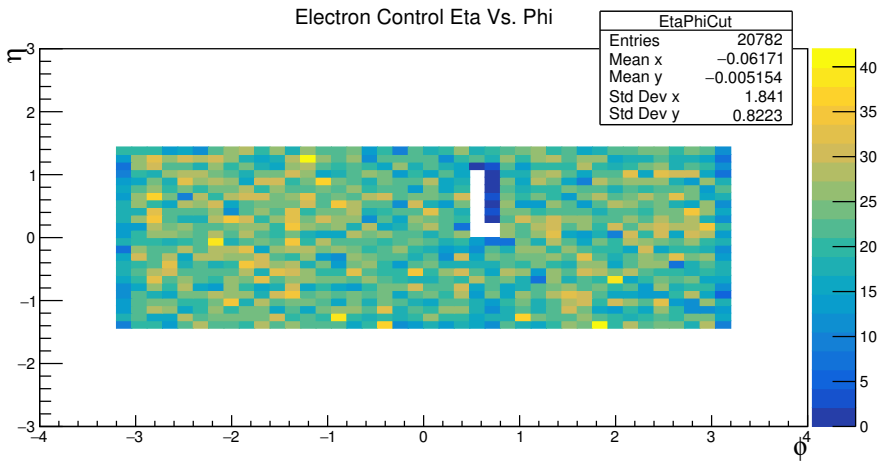

Figure 11: The η-ϕ distribution of the electron candidates.

4.2.2 $W\gamma \to e\nu\gamma$

For this region, a single electron meeting selection criteria must exist in tandem with a candidate photon as a separate object. Here, we do not require muon vetoes, nor do we require any cuts like that of the candidate sample. A quantity must be defined for this region known as recoil U, which will be cut on in this region and the Zγ region. Recoil is defined below in Equation (4).

$$\vec{U} = \vec{E_t^{miss}} + \vec{P}_t \tag{4}$$

$$U = \sqrt{(\vec{E_t^{miss}})^2 + (\vec{P}_t)^2} \tag{5}$$

The magnitude of this vector sum is then required to be greater than the E_t^{miss} cut on the candidate sample. Further, the electron must pass a P_t cut, a cut on the transverse mass, and a cut on the E_t^{miss} of these events. In addition, the electron has to pass the tight electron ID and only the electron selected can be the tight electron to ensure that this event has a reliable single electron candidate characteristic of the Drell-Yan event. This means only one of the event electrons passes the tight requirement. A summary of the exact cuts is given in Table 7 below, where the number of events that pass each cut is listed.

Cut	Number of events
$P_{t,ele} > 30GeV$	4426705
Tight Electron	1967993
Only one Tight Electron	1790160
Candidate Photon Exists in Event	221
$M_{trans} > 160GeV$	119
$U > 110GeV$	118
$E_t^{miss} > 50GeV$	118
Wγ Events (Eta/Phi Cut)	106

Table 7: Summary of cuts, and cut flow table for the Wγ control region.

For these Wγ candidates, the following plots display the distributions for their transverse energies, transverse masses, η/ϕ, and recoil. The transverse energies are given in Figure 12, the transverse masses in Figure 13, the η-ϕ distribution in Figure 14 and the recoil distribution in Figure 15.

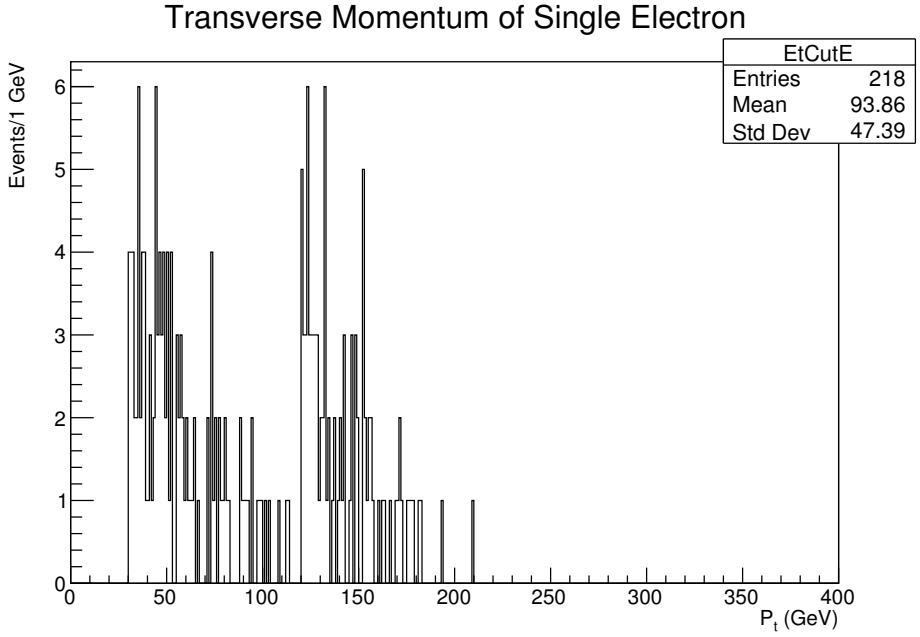

Figure 12: The E_t distribution of the Wγ candidates.

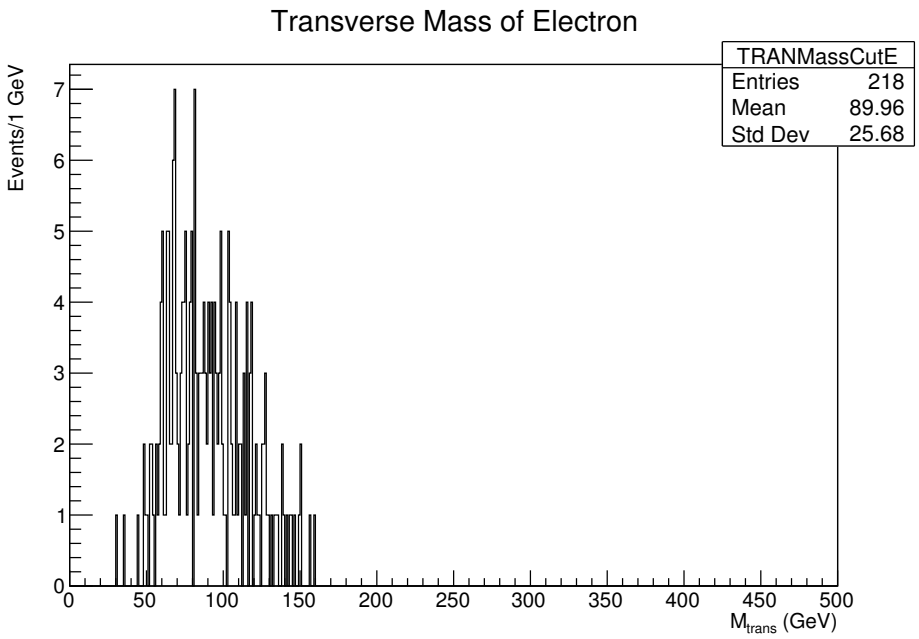

Figure 13: The M_{trans} distribution of the Wγ candidates.

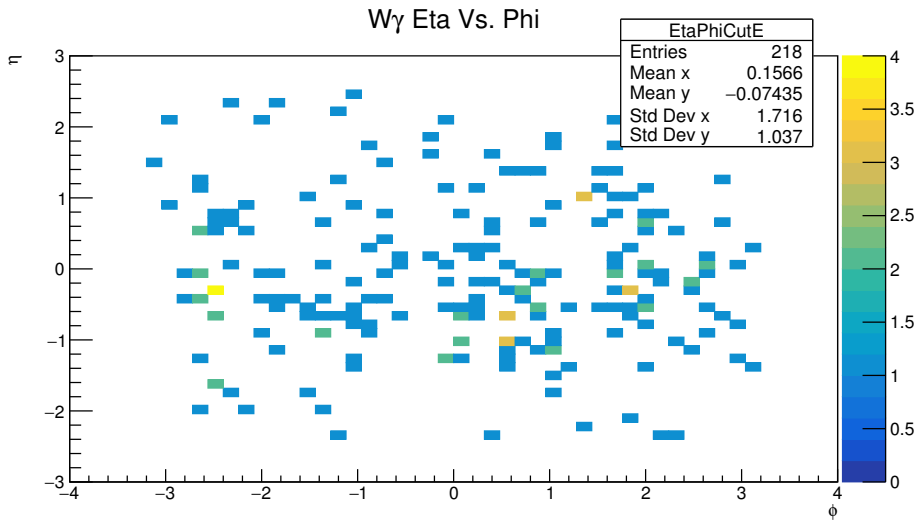

Figure 14: The η-ϕ distribution of the single electron in the Wγ candidates.

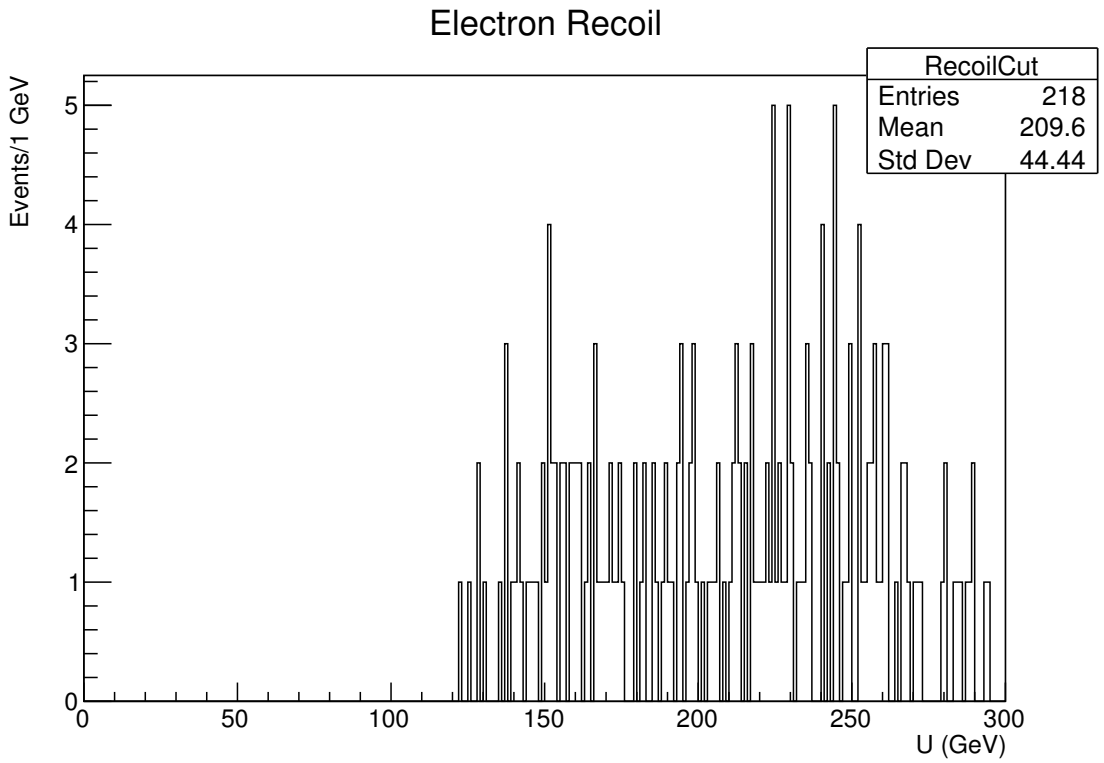

Figure 15: The recoil U distribution of the Wγ candidates.

4.2.3 $Z\gamma \to ee\gamma$

The Zγ requires two electrons that meet selection criteria. These requirements are similar to those of the Wγ region. The two electrons must be oppositely charged and either both must pass tight requirements or one must be tight and the other loose. A summary of the exact cuts is given in Table 8 below, where the number of events that pass each cut is listed.

Cut	Number of events
Exactly 2 Electrons	17968508
$P_{t,ele} > 30GeV$	4426705
Tight First Electron	1967993
Loose and Oppositely Charged Second Electron	224128
Candidate Photon Exists in Event	12
$60GeV < M_{inv} < 120GeV$	5
$U > 110GeV$	3
Zγ Events	3

Table 8: Summary of cuts, and cut flow table for the Zγ control region.

Unfortunately, this is not a sufficient number of events to examine for this analysis. As such, this region will not be pursued and suggestions for future studies will be given in the conclusion.

5 Analysis Using Track Multiplicity

The track multiplicity ξ was not calculated in a straightforward manner. The track information was not stored in the data that was used for this project, thus a unique way of calculating and viewing track distributions had to be implemented. Here, three important variables were used related to the jets of the event: number of jets N_{jets}, number or charged particles in the jets N_{CH}, and the P_t of the leading track within the jets. It is also required that each jet is a $\Delta R > 0.4$ away from the candidate as to ensure that it is not the same object. From this criteria, each of the variables were plotted for the candidate sample and the control regions. These plots were then normalized so that the shapes could be compared. The plots are given in the following sections.

The leading track P_t is used in a very different way. First, the P_t was binned in non-uniform bins. These bins were made this way as a way to sufficiently to probe this space and are shown in Table 9, which will be useful in reading the next section. From there, each event had their tracks binned in this way. Then, a count was taken of how many fell into these bins per event. This number was then used to fill a multiplicity histogram for each P_t bin. This results in 19 histograms per region, where each histogram represents a different P_t slice.

Bin	P_t Range (GeV)
1	0-3
2	3-6
3	6-10
4	10-20
5	20-40
6	40-70
7	70-100
8	>100

Table 9: Table of multiplicity P_t bins.

5.1 Jets and Charged Hadrons

Below are the plots for N_{jets} and N_{CH} for the candidate sample, electron control region, and the $W\gamma$ region in Figures 16 and 17.

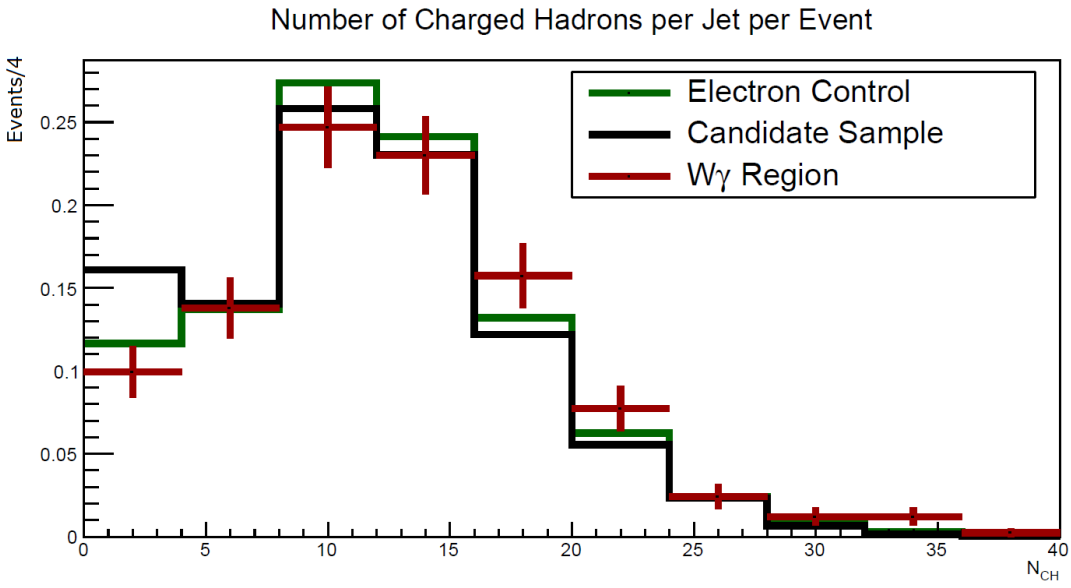

Figure 16: The distribution of N_{CH} per event for all regions.

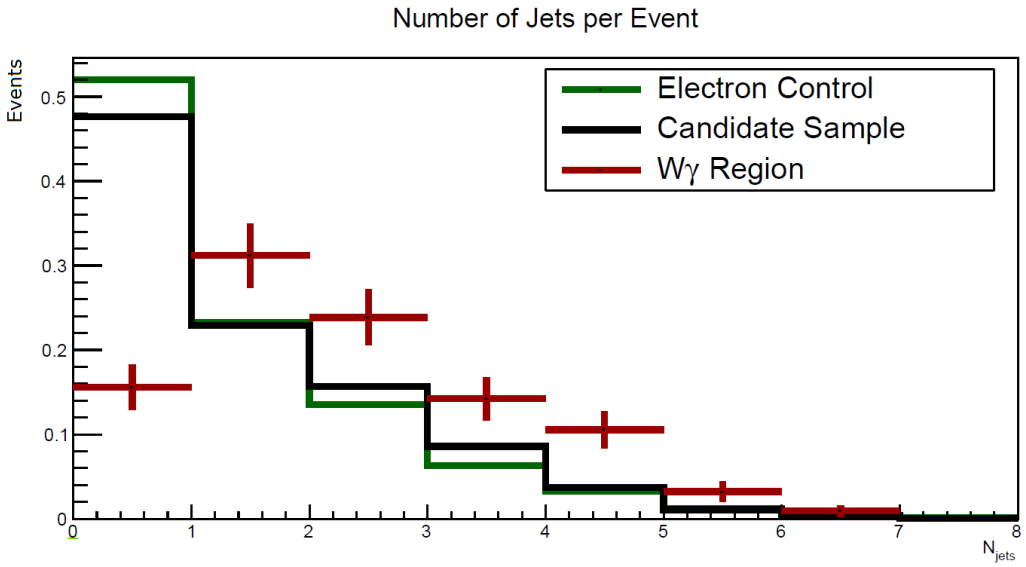

Figure 17: The distribution of N_{jets} per event for all regions.

5.2 Normalized Multiplicity Plots By P_t Slice

The results of plotting ξ by P_t slice are given in this section. These plots were normalized by the number of events in the specified region. This was done so that comparisons could be made by analysis of shape. The plots were overlayed for each bin to also allow for comparisons. All 8 plots made are given below.

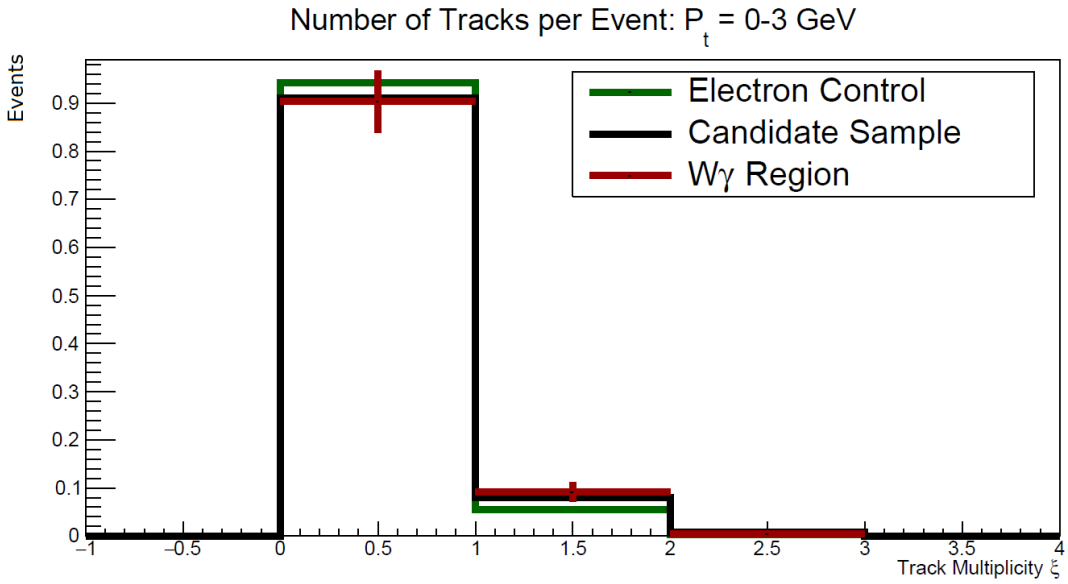

Figure 18: The ξ distributions for the first P_t bin. The green corresponds to the electron control, red to Wγ, and black to the candidate sample.

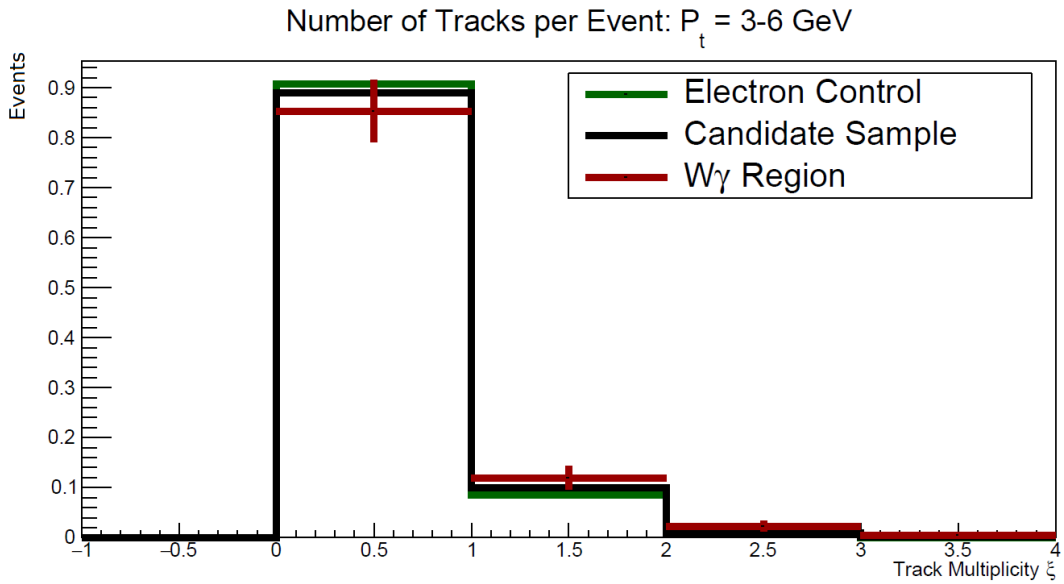

Figure 19: The ξ distributions for the second P_t bin. The green corresponds to the electron control, red to Wγ, and black to the candidate sample.

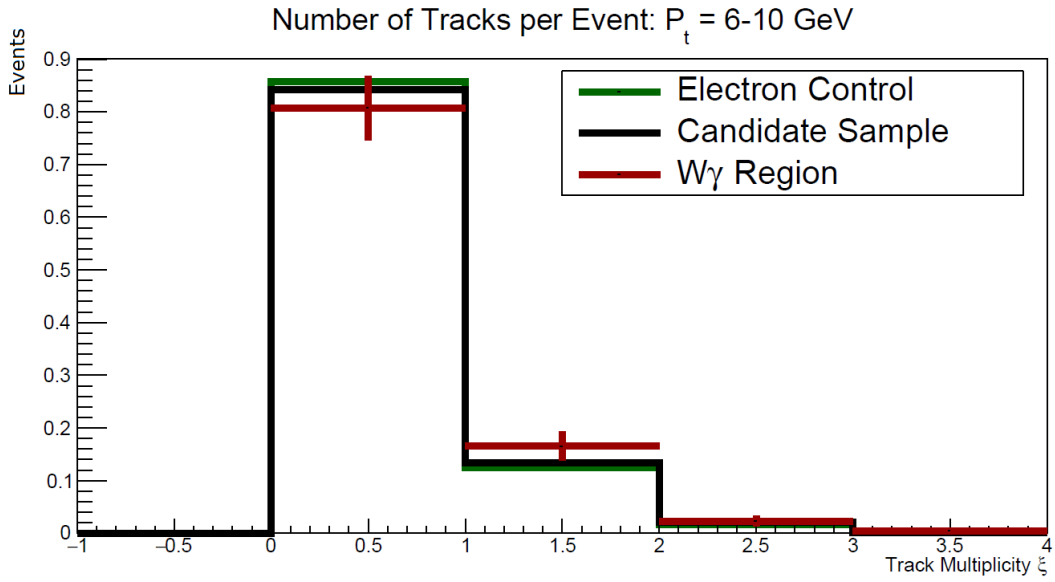

Figure 20: The ξ distributions for the third P_t bin. The green corresponds to the electron control, red to Wγ, and black to the candidate sample.

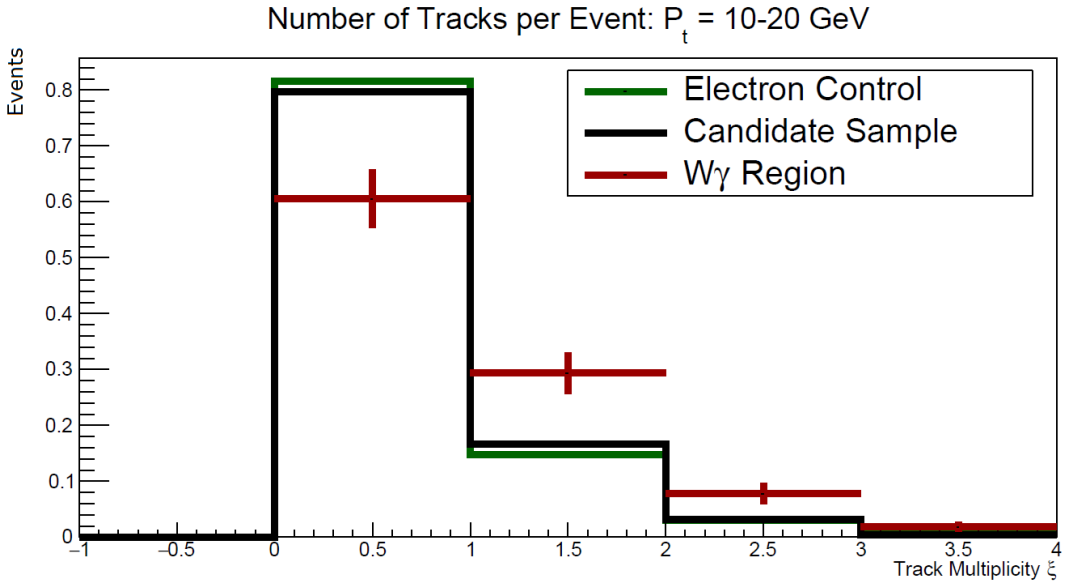

Figure 21: The ξ distributions for the fourth P_t bin. The green corresponds to the electron control, red to Wγ, and black to the candidate sample.

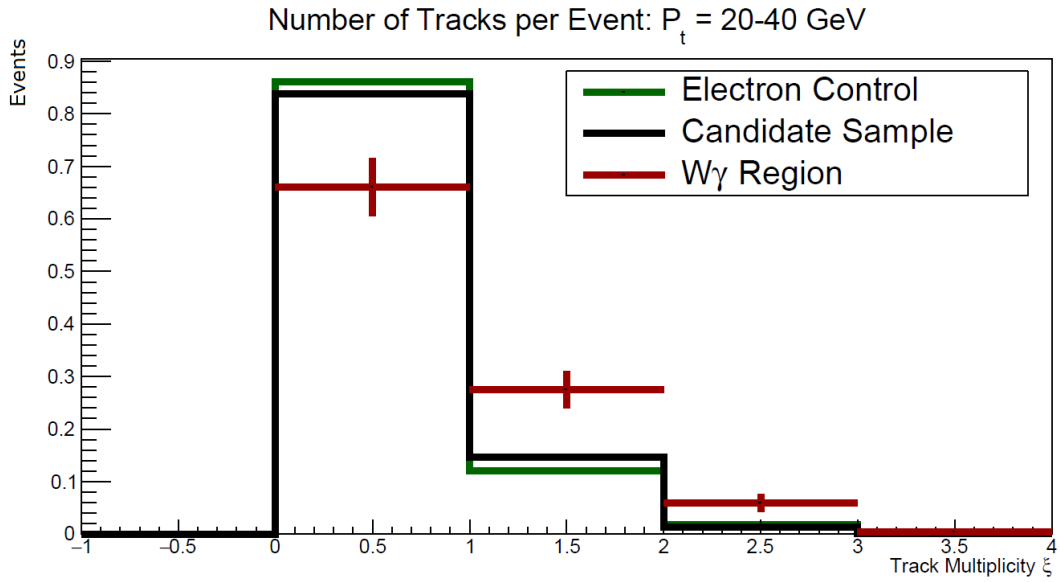

Figure 22: The ξ distributions for the fifth P_t bin. The green corresponds to the electron control, red to Wγ, and black to the candidate sample.

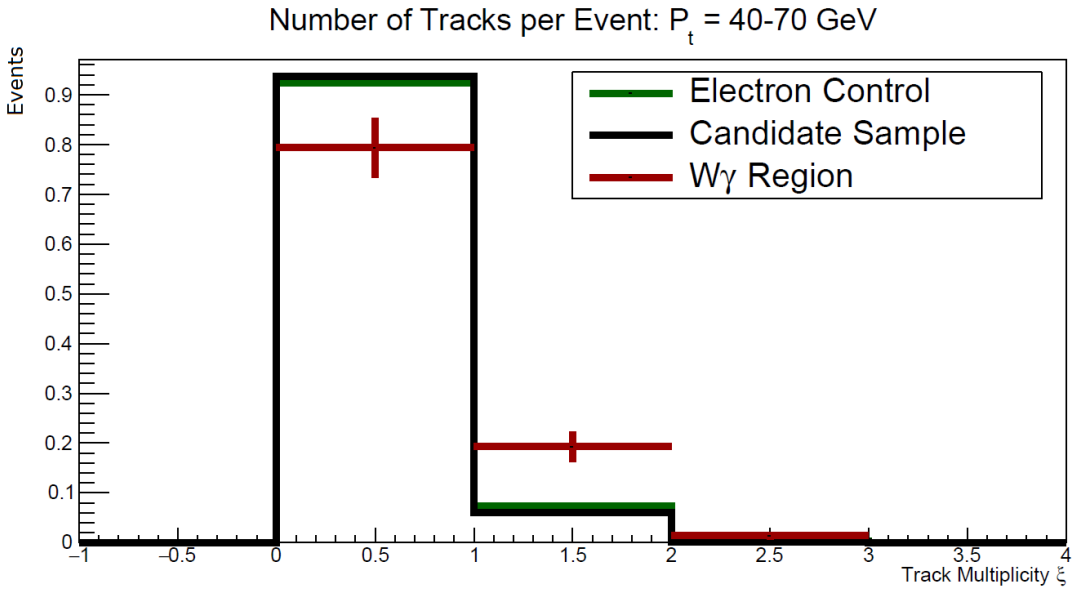

Figure 23: The ξ distributions for the sixth P_t bin. The green corresponds to the electron control, red to Wγ, and black to the candidate sample.

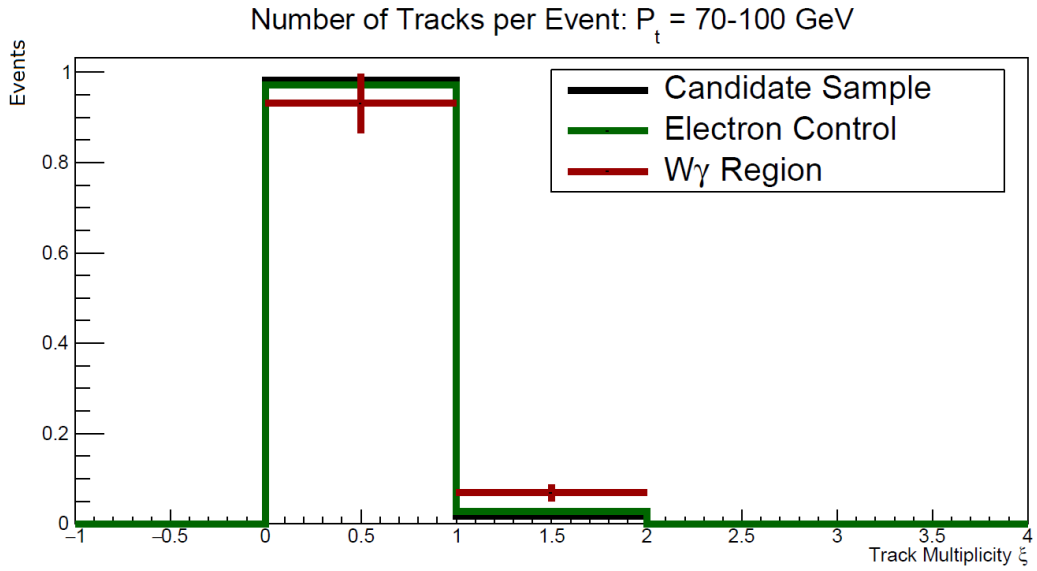

Figure 24: The ξ distributions for the seventh P_t bin. The green corresponds to the electron control, red to Wγ, and black to the candidate sample.

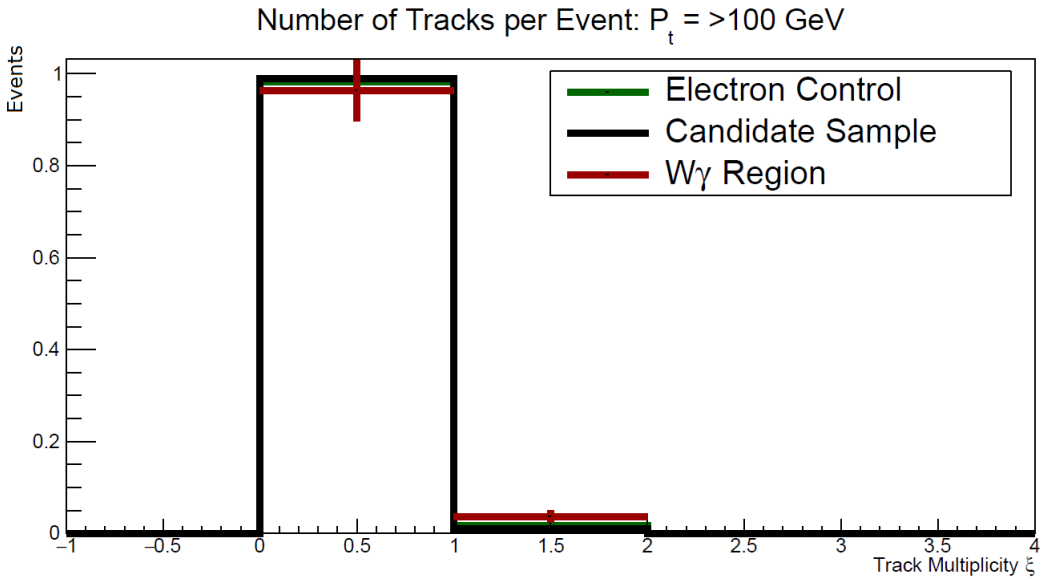

Figure 25: The ξ distributions for the eighth P_t bin. The green corresponds to the electron control, red to Wγ, and black to the candidate sample.

5.3 Comparisons

For the comparisons, χ^2 tests were made between the control regions as these are what one really wants to compare. They are given in Table 10 below.

Bin	chi^2 per degree freedom Value
1	0.0532736
2	0.0573027
3	0.0794589
4	0.162396
5	0.170895
6	0.170895
7	0.170895
8	0.0380886

Table 10: Table of χ^2 values by bin.

Quite interestingly, the candidate sample is not very similar to the Wγ control region but very similar to the electron control region. The goal of this study is not to determine any statistical differences between the three regions, or even the control regions themselves. However, it can be said that the control regions do differ from one another which can be seen in the ξ, N_{CH}, and N_{jets} distributions. In the best case, the control regions would be similar to each other and different from the candidate sample. The comparisons here yield a mixed case where the control regions are not always similar and the candidate is not different from both control regions. This is why low-mass splitting SUSY was chosen for this test, it was expected that the SUSY candidate events would have different distributions than the standard model control regions. Instead, it was found that the electron region is similar to the candidate sample, for the most part, and these both differ from the Wγ region. There are places where the Wγ region differs from the candidate sample, so there is some hope for this method. There always seems to be an excess in the ξ=2 bin for the histograms shown in the previous section. Particularly, in bins 4,5, and 6 the Wγ appears to start differing greatly. While this is not very conclusive for this study, it may hint at something in the future with more data. This method is not quite unviable yet.

6 Results and Conclusion

The ultimate result of this study is that track multiplicity has potential, but no substantial proof or disproof of this "proof of concept" was found. There is no proof in these results, as there are no significant deviations from one region to the next in terms of track distributions. This is especially true of the electron control region and the candidate sample. However, there also appears to be no disproof of this method either. This comes from the slight deviations between the $W\gamma$ region and the candidate sample. While the electron sample does not seem to deviate at all, the $W\gamma$ appears to deviate a bit in the ξ=2 bins of the plots. This means this method has some amount of viability and should be much further investigated.

Further investigation should also be prompted by some choices of this project. First, a proxy for the actual track multiplicity had to be used. This proxy was the number of lead tracks within the jets. However, this information may not give the best insight as the jets only seem to differ between the candidate sample and the $W\gamma$ region. Perhaps there is some bias from using the jets that was not thought of. Further, the data regions themselves were not exactly what was expected. the $W\gamma$ region was much smaller than in previous studies, and the $Z\gamma$ region was almost non-existent. This study would also benefit from more data, especially considering how rare the $W\gamma$ and $Z\gamma$ events are. Both events are quite rare.

All in all, the work done in this project failed to prove the use of track multiplicity as a valid method of background analysis, but it also failed to disprove this as a valid method. If anything, this has led to more questions about the data set and curiosity in what this type of study would look like on a larger scale. For example, why is the Wγ so different from the electron control and why is the electron control so similar to the candidate sample? More investigations certainly needs to be done. Further, there is still a possibility that a method of this kind could work, it just needs a lot more development before it can be put to use in the future.

References

[1] Amit Chakraborty, Sabyasachi Chakraborty and Tuhin S. Roy,
Chasing New Physics in Stacks of Soft Tracks
Department of Theoretical Physics, Tata Institute of Fundamental Research, Mumbai 400005, India, September 25, 2018
https://arxiv.org/pdf/1606.07826.pdf

[2] Sabyasachi Chakraborty,Saurabh Niyogi, K. Sridhar,
Constraining compressed versions of MUED and MSSM using soft tracks at the LHC , July 19, 2017.
https://arxiv.org/pdf/1704.07048.pdf

[3] **"Search for new physics in final states with a single photon and missing transverse momentum in proton-proton collisions at $\sqrt{s} = 13$ TeV" (primary authorship)**
A. M. Sirunyan *et al.* [CMS Collaboration].
arXiv:1810.00196 [hep-ex]
DOI:10.1007/JHEP02(2019)074
JHEP **1902**, 074 (2019)
CMS-EXO-16-053, CERN-EP-2018-248
http://inspirehep.net/record/1696608

[4] Davis,Siona
Interactive Slice of the CMS detector , August 03, 2016.
https://cds.cern.ch/record/2205172

[5] Tamas Almos Vami* for the CMS Collaboration
Calibration and performance of the CMS pixel detector in LHC Run 2 , September 9,2019.
arXiv:1909.12920v1 https://pos.sissa.it/

[6] CERN
CMS ECAL during construction. , 2020.
http://cms.web.cern.ch/news/electromagnetic-calorimeter

[7] Searching for dark matter in the Large Hadron Collider datasets
Showers in the Detectors , 2020.
https://lavanya.ai/2019/05/31/searching-for-dark-matter/

[8] 3D axis with spherical coordinates and CMS coordinate system
CMS Coordinate System , 2020.
https://wiki.physik.uzh.ch/cms/latex:tikz

A The Abnormality in the η - ϕ Distributions

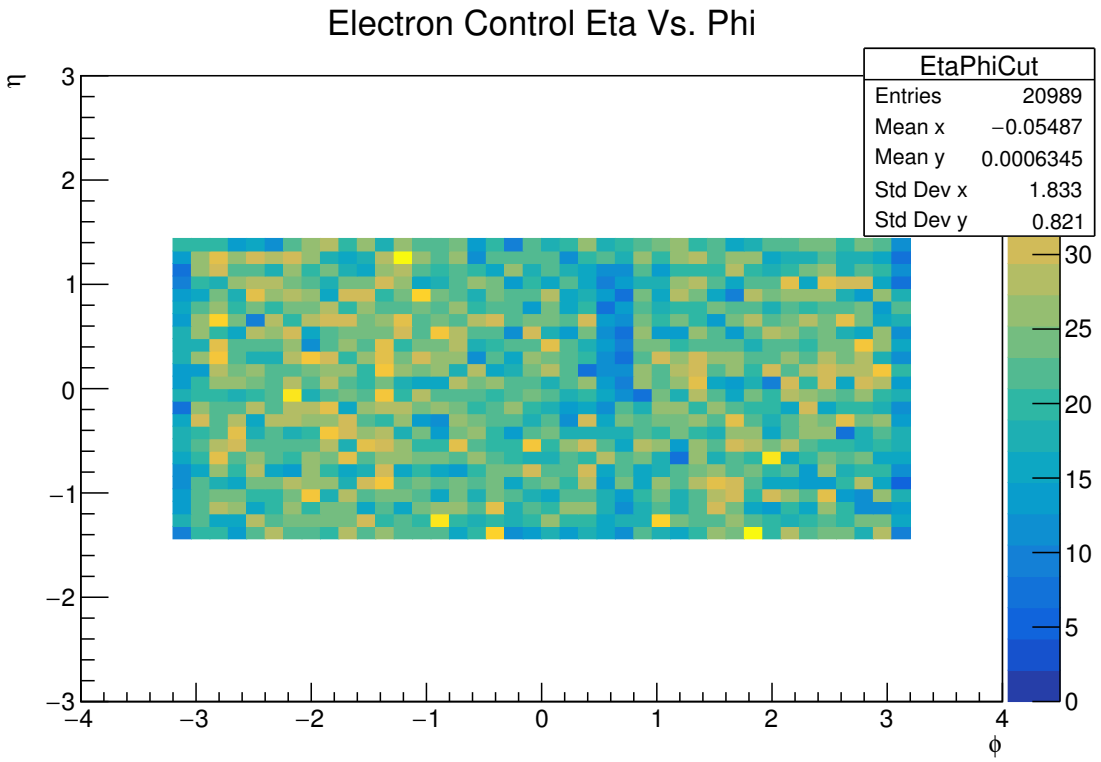

Figure 26: The lack of photons in the electron control region.

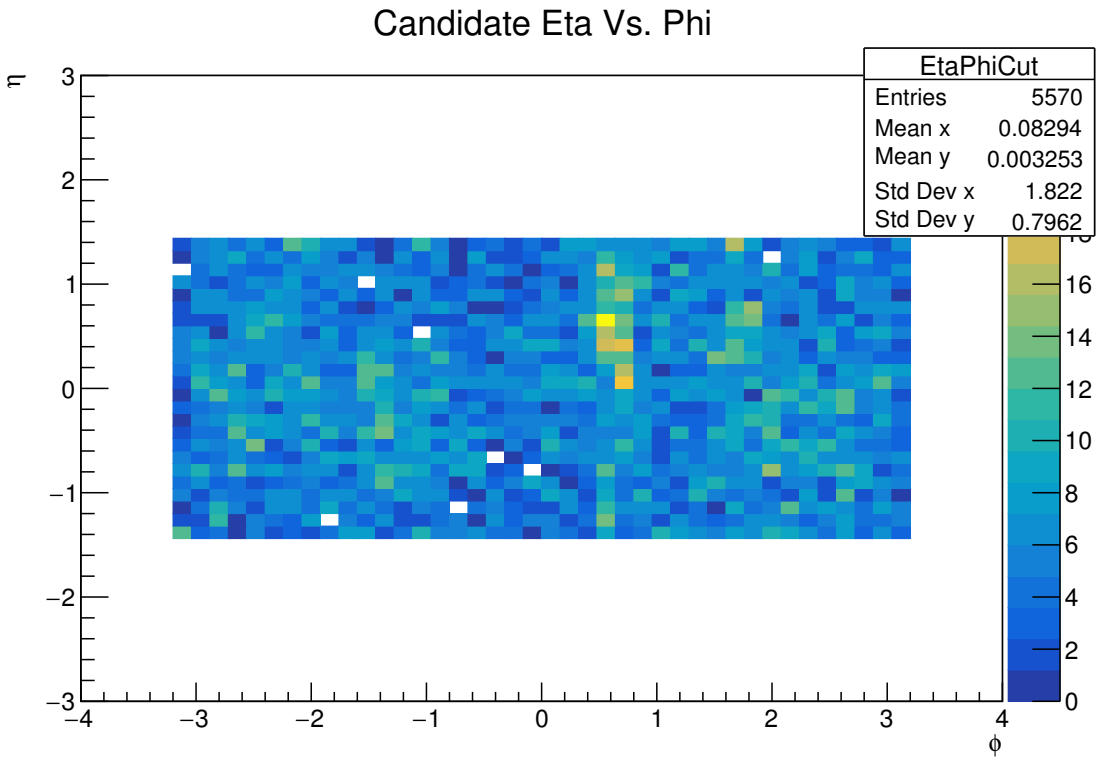

Figure 27: The excess of photons in the candidate sample.